# Dissecting the Photoprotective Mechanism Encoded by the *flv4-2* Operon: a Distinct Contribution of Sll0218 in Photosystem II Stabilization

Luca Bersanini[1], Yagut Allahverdiyeva[1], Natalia Battchikova[1], Steffen Heinz[2], Maija Lespinasse[1], Essi Ruohisto[1], Henna Mustila[1], Jörg Nickelsen[2], Imre Vass[3], Eva-Mari Aro[1*]

[1] Department of Biochemistry, Molecular Plant Biology, University of Turku, FI-20014 Turku, Finland

[2] Molecular Plant Sciences, Ludwig-Maximillians-Universität München, Biozentrum, Grosshaderner Straße 2–4, 82152 Planegg-Martinsried, Germany

[3] Institute of Plant Biology, Biological Research Centre of the Hungarian Academy of Sciences, P.O. Box 521, H-6701 Szeged, Hungary

***Corresponding author:** Prof. Eva-Mari Aro

Address: Molecular Plant Biology, Department of Biochemistry, University of Turku, FI-20014, Turku, Finland

e-mail:evaaro@utu.fi

**Running title:** Roles of Flv2/Flv4 and Sll0218 in photoprotection

## ABSTRACT

In *Synechocystis* sp. PCC 6803, the *flv4-2* operon encodes the flavodiiron proteins Flv2 and Flv4 together with a small protein, Sll0218, providing photoprotection for Photosystem II (PSII). Here, the distinct roles of Flv2/Flv4 and Sll0218 were addressed, using a number of *flv4-2* operon mutants. In the Δ*sll0218* mutant, the presence of Flv2/Flv4 rescued PSII functionality as compared to Δ*sll0218-flv2*, where neither Sll0218 nor the Flv2/Flv4 heterodimer are expressed. Nevertheless, both the Δ*sll0218* and Δ*sll0218-flv2* mutants demonstrated deficiency in accumulation of PSII proteins suggesting a role for Sll0218 in PSII stabilization, which was further supported by photoinhibition experiments. Moreover, the accumulation of PSII assembly intermediates occurred in Sll0218-lacking mutants. The YFP-tagged Sll0218 protein localized in a few spots per cell at the external side of the thylakoid membrane, and biochemical membrane fractionation revealed clear enrichment of Sll0218 in the PratA-defined membranes, where the early biogenesis steps of PSII occur. Further, the characteristic antenna uncoupling feature of the Δ*flv4-2* operon mutants is shown to be related to PSII destabilization in the absence of Sll0218. It is concluded that the Flv2/Flv4 heterodimer supports PSII functionality, while the Sll0218 protein assists PSII assembly and stabilization, including optimization of light harvesting.



## KEYWORD INDEX

Photosynthesis, cyanobacteria, Photosystem II repair, flavodiiron proteins, photoprotection

## INTRODUCTION

The oxygenic photosynthetic machinery of cyanobacteria is sensitive to environmental changes occurring in light intensity and temperature as well as to fluctuations in availability of nutrients. In particular, the effects of inorganic carbon fluctuations have been extensively studied. When the $CO_2$ concentration is high (HC), the Calvin-Benson-Bassham (CBB) cycle becomes an efficient sink for the electrons produced by the water splitting activity of PSII and cyanobacteria do grow faster (MacKenzie et al., 2004). However, during the shift to air level $CO_2$ concentrations (low $CO_2$, LC) the photosynthetic reactions are constrained: $CO_2$ becomes a limiting factor, slowing down the efficiency of CBB cycle and causing an over-accumulation of electrons in photosynthetic electron transfer chain (ETC). The strong expression of carbon concentrating mechanisms (CCMs) in cyanobacteria concentrates $CO_2$ around Rubisco and promotes cyclic electron transfer (CET) to enhance ATP production (for review, see Kaplan and Reinhold, 1999; Badger and Price, 2003; Price et al., 2008). $CO_2$ limitation also inhibits the repair of PSII since the increase of ROS production negatively affects the synthesis of D1 protein (reviewed in Nishiyama and Murata 2014). Similarly, high light (HL) intensities also cause an over-reduction of the photosynthetic electron carriers in the thylakoid membrane (TM) and are particularly damaging when combined with LC condition.

Apart from CCMs, different strategies are utilized by cyanobacteria in order to counteract the effects of inorganic carbon limitation and high light intensities. In particular, the upregulation of alternative electron transfer routes dissipate the excess of electrons in ETC, thus protecting the photosystems against photodamage. Recently the role of flavodiiron proteins (FDPs), originally called A-type flavoproteins or Flvs (Wasserfallen et al., 1998, Helman et al. 2003), has been assessed in these circumstances (Zhang et al., 2012; Allahverdiyeva et al., 2011; 2013; Bersanini et al., 2014; Chukhutsina et al., 2015).

FDPs are widespread among strict and facultative anaerobic bacteria and some eukaryotic protozoa, where they organize in homodimeric or homotetrameric forms (Vicente et al., 2008a, 2009). FDPs in these organisms function in $O_2$ and/or NO detoxification (Vicente et al., 2008b). FDPs found in cyanobacteria and some photosynthetic eukaryotes have a unique domain composition, which

theoretically allows NAD(P)H oxidation to be coupled with $O_2$ reduction in the same enzyme. *Synechocystis* sp. PCC 6803 (hereafter *Synechocystis*) contains four FDPs encoded by the *sll1521* (*flv1*), *sll0219* (*flv2*), *sll0550* (*flv3*), and *sll0217* (*flv4*) genes. *In vivo*, the presence of both Flv1 and Flv3 is a prerequisite for a Mehler-like reaction occurring at downstream of PSI (Helman et al., 2003; Allahverdiyeva et al., 2013; Mustila et al., 2016). In this process the Flv1 and Flv3 proteins donate electrons to $O_2$, similar to that in the chloroplast Mehler reaction but, importantly, ROS are not produced in the FDP-mediated reaction (Vicente et al., 2002). Under inorganic carbon starvation, about 60% of the electrons deriving from PSII activity can be redirected to Flv1/Flv3-mediated Mehler-like reaction (Allahverdiyeva et al., 2011). The Flv1 and Flv3 proteins are particularly important in fluctuating light conditions by protecting PSI against damage (Allahverdiyeva et al., 2013), yet also the Flv3 homo-oligomer has a distinct but still poorly characterized role (Hackenberg et al. 2009; Mustila et al., 2016). Further, an additional copy of Flv3 present in heterocysts of *Anabaena* sp. PCC7120 (Ermakova et al., 2013) preserves an $O_2$-free environment necessary for nitrogen fixation (Ermakova et al., 2014). Flv1 and Flv3 homologues are also found in algae and lower plants. In *Chlamydomonas reinhardtii* FDPs homologues facilitate the acclimation to anoxia during hydrogen photoproduction conditions (Jokel et al., 2015).

The *flv4-2* operon encodes Flv2 and Flv4, together with a small Sll0218 protein. Importantly, the *flv4-2* operon is highly induced in LC and HL conditions (Zhang et al., 2009) and it is strongly conserved in $\beta$-cyanobacteria (Zhang et al., 2012; Allahverdiyeva et al., 2015). Flv4 and Flv2 proteins form a heterodimer that localizes in cytoplasm but also has a high affinity to membrane in the presence of cations (Zhang et al., 2012). Sll0218, the 19kDa protein encoded by the *flv4-2* operon, locates in the membrane fraction and forms a high molecular mass complex in association with unknown partners (Zhang et al., 2012). The *flv4-2* operon-encoded proteins have a crucial role in photoprotection of PSII (Zhang et al., 2009, 2012; Bersanini et al., 2014). Overexpression of the *flv4-2* operon stimulates the oxidation of the PQ pool, concomitantly decreasing the production of singlet oxygen in PSII (Bersanini et al., 2014). Likewise, the expression of the operon increases charge separation kinetics of PSII by a slight increase of the redox potential of $Q_B$ (Chukhutsina et al., 2015). Further, the deletion of the *flv4-2* operon

hampers the accumulation of PSII dimers (Zhang et al., 2012) and a detachment of about 20% of phycobilisome antennae (Chukhutsina et al., 2015). Despite accumulating evidence for the photoprotective function of the *flv4-2* operon, its action mechanism is not yet clearly understood. In particular, the function of each single protein of the operon has been difficult to dissect due to the structure of the operon (order of the genes: *flv4-sll0218-flv2*). Here, with the use of different *flv4-2* operon mutants, we demonstrate that the Sll0218 protein resides in specific cell compartments where photosynthetic complexes are assembled, and it is involved in the stabilization of PSII assembly intermediates. In the absence of Sll0218, PSII assembly intermediates are accumulating, but the degradation of PSII subunits is not affected. Further, by increasing PSII stability, the Sll0218 protein is also responsible for efficient energy transfer from PBS to PSII reaction centers.

## MATERIALS AND METHODS

### Cyanobacterial strains and growth conditions

Wild type (WT) *Synechocystis* sp. PCC 6803 (glucose-tolerant strain, Williams, 1988) and mutant strains were grown at 30°C in BG-11 medium (Allen, 1968) supplemented with 20 mM HEPES-NaOH (pH 7.5). Cells were illuminated with white fluorescent light (L 30W/865 Osram) with intensity of ~50 µmol photons $m^{-2}$ $s^{-1}$ (Growth Light: GL); higher light intensities were used for other experiments (500, 1000 µmol photons $m^{-2}$ $s^{-1}$: HL). The cultures were cultivated in Erlenmeyer flasks shaking at 120 rpm. In LC conditions, normal air was used, and $Na_2CO_3$ was omitted from the culture ingredients. During physiological experiments, cells were grown for 5 days starting from $OD_{750}$=0.1 and finishing at $OD_{750}$=1.0-1.5. Before biophysical experiments, cells were resuspended in fresh BG-11 medium and adjusted to the same Chl concentration (5 µg $mL^{-1}$ if not stated otherwise). The Chl concentration was determined in 90% methanol by absorbance measurement at 665 nm and calculated with the extinction coefficient of 78.74 L $g^{-1}$ $cm^{-1}$ (Meeks and Castenholz 1971). The Δ*sll0218-flv2* strain was described in Helman et al. (2003), the Δ*flv2*, and Δ*flv4* strains in Zhang et al. (2012) and the OE strain in Bersanini et al. (2014). To create a mutant lacking only Sll0218, the Δ*sll0218-flv2* cells were transformed with self-replicating plasmid pVZ-*flagflv4* including the original *flv4* promoter region, as described in Zhang et al.

(2012), thus introducing into cells the *flv4* gene. After complementation with *flagflv4,* the *flv2* gene was reintroduced by transformation with a plasmid (modified pPSBA2KS, Lagarde et al., 2000) containing the *flv2* gene under the control of the *psbA2* promoter. The *flv2* construct was integrated into the chromosome by replacing the *psbA2* gene. Deletion of the *psbA2* gene does not generally harm the cells due to concomitant adjustment of the expression of the *psbA3* gene that encodes the D1 protein identical to that encoded by the *psbA2* gene (Mohamed et al., 1993). To obtain the Sll0218-eYFP mutant, *sll0218* ORF together with the upstream region was amplified by PCR using FwI-*Sal*I (5′-gctcagtcgacgttcaccttctacctgggatt-3′) and RvI-BamHI (5′-catgcggatcccctcctgagcctcctccaattgatggggactccttacc-3′) primers followed by restriction with *Sal*I and *BamH*I. The region downstream to *sll0218* (‘*sll0218* downstream’) was amplified using FwII-*EcoR*I (5′-cgaccgaattcttatcttgaccatccccgct-3′) and RvII-SpeI (5′-gacctactagtcaaagtaaaaacggcgatcg-3′) primers followed by restriction with *EcoR*I and *Spe*I. The pEYFP-$His_6$-$Spc^R$ plasmid described in Birungi et al. (2010) was digested in order to obtain a *Sal*I-*Spe*I vector and a *BamH*I-*EcoR*I fragment containing YFP ORF and the spectinomycin/streptomycin resistance cassette. The four fragments (*sll0218* ORF + BamHI-EcoRI fragment + *sll0218* downstream + SalI-SpeI vector) were ligated together, and the obtained pSll0218-eYFP plasmid was used for transformation of *Synechocystis* WT. A schematic map of pSll0218-eYFP plasmid is reported in Supplemental Figure S1. The accuracy of plasmid assemblies was verified by sequencing. Segregation to homogeneity of the obtained mutants was confirmed by PCR analysis and immunoblotting.

**Oxygraphic analysis by Clark-type electrode**

Steady state $O_2$ evolution was determined with a Clark-type $O_2$ electrode (DW1, Hansatech) at 30°C under saturating white light with intensity of 1,000 µmol photons $m^{-2}$ $s^{-1}$. The PSII electron transport rates were defined in the presence of an artificial electron acceptor, 2 mM 2,6-dimethyl-*p*-benzoquinone (DMBQ).

**Fluorescence analysis**

A pulse amplitude modulated fluorometer Dual-PAM-100 (Walz, Effeltrich, Germany) was utilized to examine Chl fluorescence *in vivo*. Red (620 nm) actinic light was applied, and cells were stirred in 1cm x

1cm cuvettes at 30°C during the measurements. Saturating pulses (red light, 5,000 µmol photons $m^{-2}$ $s^{-1}$, 300 ms) were used to transiently close all PSII centers. The effective yield of PSII, Y(II)= ($F_m'$-$F_s$)/ $F_m'$, was measured from the cells illuminated with an actinic light intensity of 120 µmol photons $m^{-2}$ $s^{-1}$ for 2 min.

Fluorescence emission spectra of intact cells at 77K were determined with a USB4000-FL-450 (Ocean Optics) spectrofluorometer. The cells were frozen in liquid nitrogen directly from the GL conditions. Fluorescence emission spectra were recorded by excitation with 580nm light obtained via interference filters 10 nm in width. Samples were adjusted to same Chl *a* concentration (5 µg $mL^{-1}$) before the measurements.

**Protein isolation, SDS-PAGE, BN-PAGE and immunodetection**

Total cell extracts as well as the soluble and membrane fractions of *Synechocystis* cells were isolated as described by Zhang et al. (2009, 2012). Proteins were separated by 12% (w/v) SDS-PAGE containing 6 M urea. Protein complexes in the membrane fractions were studied by Blue Native (BN)-PAGE, according to Zhang et al. (2012) using gradient polyacrylamide gels (4.5%–12%). For electrophoresis in the second dimension (2D), a strip of the BN gel was incubated in the Laemmli SDS sample buffer containing 5% β-mercaptoethanol and 6 M urea for 1 h at 25 °C. The strip was then placed onto a 1-mm-thick 12% SDS polyacrylamide gel with 6 M urea (Laemmli 1970). After electrophoresis, the proteins were transferred to a PVDF membrane (Immobilon-P; Millipore) and examined with protein-specific antibodies.

**Isolation of membrane fractions**

WT cells were washed with 5mM Tris buffer (pH 6.8), and resuspended in buffer I (10 mM Tris pH 6.8, 1 mM phenylmethylsulfonyl fluoride (PMSF), 600 mM sucrose, 5 mM EDTA, 0.2% lysozyme). The suspension was incubated for 2 h at 30°C and shaken; then it was washed twice in buffer II (20mM Tris, 1mM PMSF). Cells were disrupted with a French Press (1200 p.s.i.) followed by the treatment with DNase I (15 min at 4°C) and centrifugation of samples (4 °C, 4500 x *g*, 10 min). The obtained supernatant was adjusted to 50% sucrose, and 10-ml of this solution was overlaid with 8 ml of 39% sucrose, 6 ml of 30% sucrose, and 8 ml of 10% sucrose (all in 10 mM Tris pH 6.8, 1 mM PMSF). Following centrifugation at 4 °C for 17 h at 135,000 x *g,* the gradient was divided into five fractions containing 10% (I), 30% (II), or 50% (V)

sucrose. To reach a higher resolution, the portion containing 39% sucrose was separated into two fractions (III and IV). The fraction V was diluted to a 20% sucrose concentration, loaded onto a linear (30% to 60%) sucrose gradient and then centrifuged for 17 h at 135,000 x *g* at 4 °C, followed by fractionation and immunodetection using anti-PratA antibodies; the presence of PratA defined the PDM (PratA-defined membrane) fractions. For more details of this procedure, see Schottkowski et al. (2009a).

**Confocal microscopy**

Fluorescence micrographs were recorded using an LSM 510 Meta confocal microscope (Carl Zeiss, Jena, Germany) with a 100x/1.4 plan apochromat oil immersion objective and an 80-µm confocal pinhole. The excitation of enhanced YFP and Chl autofluorescence were achieved respectively with the argon ion laser (514 nm) and the helium laser (543 nm). Enhanced YFP fluorescence emission was collected with a 515nm dichroic mirror and a band pass filter of 535-590 nm. Chl autofluorescence was obtained through a 545nm dichroic mirror and a long pass filter of 560 nm. ImageJ software was used for image analysis together with radial profile plot written by Paul Baggethun. Chl autofluorescence was used to describe the cell geometry in the determination of radial fluorescence profiles for cells. According to Sacharz et al., (2015), a circular area was individuated manually for each cell, and a radial distribution was determined by summing the fluorescence values at each given distance from the center. Distributions were normalized to the cell radius.

**RESULTS**

**Phenotype of different *flv4-2* operon mutants**

Differential expression of proteins encoded by the *flv4-2* operon in mutants utilized here is shown in Figure 1A. The Δ*flv2* mutant does not express the Flv2 protein and retained only a low amount of Flv4, whereas the Sll0218 protein accumulated to WT levels (Zhang et al., 2012). The Δ*sll0218-flv2* mutant lacks both Sll0218 and Flv2, and possess only a low amount of Flv4 (Zhang et al., 2012). Since the gene order of the *flv4-2* operon is *flv4-sll0218-flv2*, a deletion mutant of only the *sll0218* gene by direct knock out would disrupt the reading frame of the operon and compromise the expression of *flv2*, thus resulting in a strain with similar features to the Δ*sll0218-flv2* mutant. Therefore, a Δ*sll0218* mutant was generated by

194 reintroducing *flv2* and *flv4* in the Δ*sll0218-flv2* mutant background. This led to accumulation of the Flv2
195 and Flv4 proteins to a similar or slightly higher levels, respectively, compared to WT and to a concomitant
196 absence of the Sll0218 protein. Since the Flv2/Flv2 and Flv4/Flv4 homodimers are not functional *in vivo*
197 (Zhang et al., 2012), a possible excess of Flv4 in Δ*sll0218* is expected not to provide any additional effect.
198 The OE strain showed overexpression of all three proteins, Flv4, Sll0218 and Flv2, encoded by the operon
199 (Bersanini et al., 2014 Figure 1A).
200 A visual phenotype of the cultures grown at 500 µmol photons $m^{-2}$ $s^{-1}$ (High Light, HL) for 6 days is
201 depicted in Figure 1B: the Δ*sll0218-flv2,* Δ*flv4* and Δ*sll0218* cultures showed a distinct yellow color
202 compared to WT. The Δ*flv2* culture showed a mix color phenotype between WT and the other deletion
203 strains, whereas the OE mutant, as shown earlier in Bersanini et al. (2014), had a darker green color than
204 WT. This was reflected in the chlorophyll (Chl) *a* content of the cultures (Figure 1C). Already in 50 µmol
205 photons $m^{-2}$ $s^{-1}$ (Growth Light, GL) all other mutants but not OE displayed a 20 to 25% decrease in Chl *a*
206 content compared to WT. When cells were grown in HL, the Δ*flv2* strain displayed a similar 20-25%
207 decrease in Chl *a* content as in GL, whereas the Δ*sll0218-flv2,* Δ*flv4* and Δ*sll0218* strains demonstrated a
208 drop in Chl *a* content to about 50% compared to WT. The OE strain showed a 30% increase in Chl *a*
209 content compared to WT (Figure 1C).

210 **Accumulation of thylakoid proteins and the PSII activity in *flv4-2* operon mutants**

211 In GL conditions, the lack of Flv2 and reduced amount of Flv4 in the Δ*flv2* mutant were accompanied by
212 30% decrease of D1 content as compared to WT. The absence of the entire operon and thus all three
213 proteins, Sll0218, Flv2 and Flv4, resulted in a 50% decrease of D1 accumulation (Δ*sll0218-flv2*, Δ*flv4*).
214 Strikingly, the absence of only the Sll0218 protein impaired D1 accumulation to the similar extent as
215 those lacking the whole operon-encoded proteins. Other PSII proteins (D2 and CP43) and the subunits
216 of the Cyt $b_6$f and PSI complexes, the Cytf and PsaB proteins, showed comparable decrease in the
217 accumulation level as the D1 protein in the different mutant strains. On the contrary, the OE strain
218 showed similar accumulation of thylakoid proteins as WT (Figure 2A).

PSII functionality was determined by PAM fluorometry as Y(II) and as a rate of oxygen evolution in the presence of 2,6-dimethyl-*p*-benzoquinone (DMBQ), which is an artificial electron acceptor (Figure 2B). The lack of all three proteins of the operon decreased Y(II) and $O_2$ evolution rate about 40-45% (Δ*sll0218-flv2,* Δ*flv4*). Importantly, the Δ*sll0218* mutant, obtained with the expression of Flv2/Flv4 in Δ*sll0218-flv2*, demonstrated only slightly lower Y(II) and PSII oxygen evolution rates (expressed on Chl *a* basis) than WT, although this difference is not statistically significant. Thus in Δ*sll0218,* compared to Δ*sll0218-flv2*, the presence of Flv2/Flv4 rescued the activity of PSII to a large extent. The Δ*flv2* mutant possessing the Sll0218 and a faint amount of the Flv4 proteins, demonstrated about 20 and 40% lower oxygen evolution rate and Y(II), respectively, as compared to WT. In contrast, the OE mutant showed 20-40% higher PSII activity than the WT (Figure 2B, Bersanini et al., 2014).

**High light susceptibility of the *flv4-2* operon mutants**

The sensitivity of the *flv4-2* operon mutants to high light was tested by determining the time course of inhibition of PSII oxygen evolution activity in the absence (photoinhibition) and presence of lincomycin (photodamage), an inhibitor of protein synthesis, thus blocking the PSII repair (Figure 3). Sensitivity of the all *flv4-2* operon deletion mutants to photoinhibition was evident especially in the beginning of the shift to HL. The OE strain was more tolerant to HL than the WT in the absence (Figure 3, Bersanini et al., 2014) and in the presence of lincomycin (Figure 3). Intriguingly, only the Δ*flv2* mutant possessing the Sll0218 protein, demonstrated less sensitivity to photoinhibition in the absence of lincomycin, upon prolonged exposure (90 min) to HL. When the high light illumination of the cells was performed in the presence of lincomycin, differences between the mutants and WT were observed only in the beginning of the high light treatment, and disappeared after 60 min exposure of cells to HL (Figure 3).

The absence of Sll0218 increased PSII photosensitivity upon longer term exposure to HL, which apparently resulted from impaired PSII assembly/repair process observed only in the absence of lincomycin. Importantly, the degradation of the D1 protein, assessed in lincomycin treated cells exposed to 1000 µmol photons $m^{-2}$ $s^{-1}$ for a maximum of 5 hours, showed no distinct pattern between the WT,

244 Δ*sll0218-flv2* and Δ*sll0218* strains (Supplemental Figure S2), thus uncoupling the function of proteins
245 encoded by the *flv4-2* operon from the degradation of the D1 protein.

246 **Accumulation of PSII assembly intermediates in the *flv4-2* operon mutants**

247 The accumulation of PSII complexes in the TM was assessed through immunoblotting of the BN-PAGE
248 gels with D1 antibodies. Beside the PSII dimer, monomer, CP47- monomer and reaction center (RC)
249 complexes, the mutants lacking Sll0218, but not the Δ*flv2* mutant (Supplemental Figure S3B), showed
250 an unusual accumulation of two small protein complexes containing the D1 protein (red arrows in Figure
251 4A and Supplemental Figure S3A), with a molecular mass slightly superior to the SbtA complex.
252 Immunoblotting of the BN-PAGE gels with antibodies specific for YCF48, a PSII assembly factor, revealed
253 a stronger accumulation of this protein in Sll0218-lacking mutants (Figure 4A, Supplemental Figure S3B)
254 whereas the OE mutant demonstrated low levels of YCF48 (Supplemental Figure S3B). Noteworthy, the
255 two closely migrating YCF48 complexes in the BN-PAGE co-migrated with the D1-containing complexes
256 mentioned above. Next, this region of protein complexes, indicated by a red rectangle in the first BN-gel
257 of Figure 4A, was subjected to SDS-PAGE in the second dimension (2D) followed by immunoblotting
258 with D1 and YCF48 antibodies. This analysis showed that YCF48 and D1 indeed belong to the same PSII
259 intermediate complex (Figure 4B). The PSII subcomplex indicated by a yellow arrow likely represents the
260 RC* (PSII reaction center complex *), localized between the CP43-less PSII monomer (CP47-RC) and PSII
261 monomeric complexes (Figure 4, Supplemental Figure S3B, Rengstl et al., 2013). RC* is composed of full
262 D1 or its intermediate form (iD1), D2, PsbI, cytb$_{559}$, YCF48, together with a Ycf39-HliD subcomplex
263 (Komenda et al., 2008; Knoppova et al., 2015). The two small PSII subcomplexes identified in the Sll0218-
264 lacking mutants and indicated by red arrows in Figure 4, possibly correspond to the RCa complexes,
265 which is a RC* devoid of Ycf39-HliD subcomplex (Knoppova et al., 2015). These complexes could not be
266 visualized with protein staining, most probably because of their low relative abundance.

267 **PSII assembly factors in the *flv4-2* operon mutants**

268 Since the assembly of PSII seemed to be malfunctioning in the *flv4-2* operon mutants, the content of a
269 number of proteins involved in PSII assembly was next addressed by immunoblotting with

corresponding antibodies. As already suggested by the BN-PAGE gels (Figure 4), the most conspicuous differences between the *flv4-2* operon mutants existed in the amounts of the YCF48 protein. In comparison to WT, the absence of Sll0218 increased the content of YCF48 to maximum of 140%, while the OE strain had only about 50% of WT YCF48 level (Figure 5A). The amount of the Sll0933 protein, a homologue of plant PAM68 (Armbruster et al., 2010), which was reported to interact with YCF48 (Rengstl et al., 2013), did not differ significantly among the *flv4-2* operon mutants. Similar constancy was observed for PratA (Figure 5A), which is responsible for the delivery of $Mn^{2+}$ ions to the precursor form of D1 (pD1) protein (Stengel et al., 2012). The levels of protochlorophyllide oxidoreductase (POR), a protein involved in Chl biosynthesis (Eckhardt et al., 2004, Schottkowski et al., 2009a), were slightly elevated in all the mutants. The protein levels of Pitt, a membrane-bound tetratricopeptide repeat protein that binds and stabilizes POR (Schottkowski et al., 2009b), and Vipp1, involved in TM maintenance (Westphal et al., 2001), were slightly lower in the *flv4-2* operon deletion mutants, compared to WT. The levels of Oxa1 protein, which supports the integration, folding, and/or assembly of precursor D1 form (Ossenbühl et al., 2006), were slightly lower in the OE mutant (Figure 5A). The accumulation of a stomatin-like protein homologue, called Phb3 (Slr1128), with unclear function in cyanobacteria, was impaired in Sll0218-lacking mutants (Supplemental Figure S4).

**Presence of *flv4-2* operon-encoded proteins in *ycf48* and *sll0933* deletion mutants**

Since the presence of PSII assembly factors differs among the *flv4-2* operon mutants, the reverse situation was also tested by assessing the contents of the *flv4-2* operon-encoded proteins in Δ*ycf48*, Δ*sll0933* and the double mutant Δ*ycf48/sll0933*. When the loading of gels was normalized to the total protein content, the D1 amounts were, as expected, lower in the PSII assembly mutants than in WT (Figure 5B, Komenda et al., 2008; Rengstl et al., 2013). Nevertheless, we could detect all the *flv4-2* operon-encoded proteins in the Δ*sll0933* mutant. In the mutants lacking YCF48, only Flv2 was detectable, Flv4 was difficult to identify possibly because of the lower quality of the antibody, but the Sll0218 protein was clearly absent (Figure 5B). More detailed characterization of the expression of the *flv4-2* operon encoded proteins was performed in the Δ*ycf48* and Δ*ycf48/sll0933* strains. Since the function of the *flv4-2* operon-encoded proteins is related to PSII, the loading of proteins in the gels was normalized to the

D1 content, according to the quantification performed in the previous experiment. With this setup, the Flv2 and Flv4 proteins could be clearly identified. Interestingly, the Sll0218 protein still remained undetected (Figure 5C).

**Localization of Sll0218 in *Synechocystis* cells**

To investigate the subcellular localization of the Sll0218 protein *in vivo*, the yellow fluorescent protein (YFP) was fused to the C-terminus of Sll0218. Subsequent immunoblottings with the Sll0218 and YFP specific antibodies confirmed the expression of the Sll0218-YFP protein, with an approximate size of ~50KDa (Supplemental Figure S5). Confocal fluorescence microscopy images revealed distribution of Sll0218-YFP in small spots in the cells (Figure 6A). The number of spots was determined to be in an average of 2.13 per cell (Figure 6B). Further comparison with the radial distributions of Chl fluorescence and Sll0218-YFP fluorescence showed that Sll0218 spots were localized mainly at the peripheral side of the Chl fluorescence patterns (Figure 6C), thus denoting the localization of the fusion proteins to the side of TM which is more in the vicinity to the cytoplasmic membrane (Mullineaux and Sarcina, 2002).
To further explore Sll0218 localization, *Synechocystis* membranes were isolated and fractionated according to Rengstl et al., (2011) and the PratA-defined membrane areas, called PDMs, were defined. PDMs are considered to be specific areas of biogenesis of photosynthetic complexes, in particular of PSII, and are located in the contact area of the TM with the cytoplasmic membrane, or around the thylakoid biogenesis centers (Stengel et al., 2012). The protein content of the PDM fraction was verified by immunoblotting with PratA, D1, PsaB, YCF48 and Sll0933 antibodies and demonstrated a typical pattern with PratA strictly accumulated in PDM fractions, D1 and YCF48 accumulated in PDM and TM fractions, while PsaB and Sll0933 represented strict TM markers (Rengstl et al., 2011). Most importantly, the Sll0218 protein was present only in the PDM fractions (Figure 6D).

**Differences in light harvesting properties of the *flv4-2* operon mutants**

To distinguish the role of *flv4-2* operon-encoded different proteins in harvesting of light energy, we recorded the fluorescence emission spectra at 77K, with an excitation at 580 nm. High F685 peak clearly distinguished the Δ*flv4* and Δ*sll0218-flv2* strains from WT, as reported also earlier (Zhang et al., 2012;

Bersanini et al., 2014). Nevertheless, the Δ*sll0218* strain also demonstrated a high F685 as compared to WT, while the Δ*flv2* strain, expressing the Sll0218 protein, had just a slightly higher F685 peak compared to that in WT.

Moreover, the minimal level of the fluorescence in the dark, the $F_0$, which is also an indication of antenna detachment (Campbell et al., 1998; Acuña et al., 2015) was clearly higher in the Sll0218-lacking mutants (Supplemental Figure S6), thus confirming that the lack of Sll0218 is the main cause for antenna detachment.

## DISCUSSION

Although the research on FDPs in oxygenic photosynthetic organisms is constantly increasing, several fundamental questions on their mode of action and reasons for arrangement in an operon still remain unclear. This is particularly the case with the *flv4-2* operon-encoded proteins and their function in photoprotection of cyanobacterial PSII ( Zhang et al., 2009, 2012; Hakkila et al., 2013; Bersanini et al., 2014; Chukhutsina et al., 2015). In this work we addressed the function of the three proteins encoded by the *flv4-2* operon, the Flv4, Sll0218 and Flv2 proteins. Towards this end, we characterized different *flv4-2* operon mutants with deficiencies or overexpression of Flv2, Sll0218 and Flv4 proteins, together or singularly, and assessed their specific significance for the functionality and turnover of PSII.

### Sll0218 contributes to stabilization of newly assembled PSII in thylakoid biogenesis centers

The Sll0218 protein encoded by the *flv4-2* operon has remained the most cryptic component of this photoprotection machinery. The partially independent function of Sll0218 from the Flv2/4 heterodimer can already be deduced from the expression pattern of the Flv2, Sll0218 and Flv4 proteins in the mutant collection used here. When the *flv2* gene is deleted (Δ*flv2* strain) also the expression of the Flv4 protein is low but the Sll0218 protein is present in the TM at WT-levels (Figure 1A). Conversely, in mutants lacking YCF48, the Flv2 and Flv4 proteins are present but the Sll0218 protein is missing (Figure 5B-C). Thus, it is highly conceivable that the presence of YCF48 is required for the specific accumulation of Sll0218. Additionally, both are membrane proteins with reported connections to PSII (Komenda et al., 2008; Zhang et al., 2012; Mabbitt et al., 2014; Chukhutsina et al., 2015). These observations prompted us to

investigate in more detail the role of the Sll0218 protein as a distinct component and separate player from that of the Flv2/Flv4 heterodimer in protection of PSII.

The fact that the lack of the sole Sll0218 protein (Δ*sll0218*) caused, under LC growth conditions, a similar deficiency in Chl *a*, PSII and other photosynthetic complexes as observed in the entire *flv4-2* operon deletion mutants (50% less PSII than in WT on protein basis) (Figure 1C) suggested a before unforeseen role for the Sll0218 protein. Despite the scarcity of PSII proteins in the absence of Sll0218, they seemed to be properly assembled as the Δ*sll0218* mutant displayed nearly WT-like PSII activity when expressed on the Chl basis. No significant compromise in the functionality of PSII in the Δ*sll0218* mutant suggested that Sll0218 may rather play a role in stabilization of PSII under repair/assembly.

To test the hypothesis of a PSII stabilization role for Sll0218, *Synechocystis flv4-2* operon mutants were shifted to HL in order to enhance PSII photoinhibition and subsequent PSII repair/assembly processes. Indeed, the mutants which lacked Sll0218 were the most sensitive to photoinhibition, as also indicated by drastic changes in the color and the Chl *a* content of the cultures (Figure 1B-C). When lincomycin was added to the cells upon exposure to HL, all *flv4-2* operon mutants displayed similar PSII inhibition kinetics from 60 min illumination onwards. Collectively, the photoinhibition experiments in the absence and presence of lincomycin support the hypothesis of the role of Sll0218 protein in the stabilization of assembly/repair of PSII. The PSII repair starts with degradation of the damaged D1 protein (Aro et al., 1993; Aro et al., 2005). This initial PSII repair phase, however, did not reveal any significant differences between the mutants. (Supplemental Figure S2), suggesting that the proteolytic degradation of D1 is not considerably affected by the presence or absence of Sll0218. Subsequent steps of PSII repair involve a co-translational incorporation of the D1 protein into partially disassembled PSII complex and subsequent reassembly of the detached proteins and cofactor components (Aro et al., 2005; Järvi et al., 2015). These assembly/repair phases of PSII have been investigated in cyanobacteria in great detail during the past few years (see reviews Komenda et al., 2012; Nickelsen and Rengstl 2013; Heinz et al., 2016).

Characterization of the *flv4-2* operon mutants with respect to PSII assembly/repair revealed two intermediate complexes containing D1 and YCF48, which specifically accumulated in the strains lacking the Sll0218 protein (Figure 4). According to the mobility in the BN-PAGE gels, these PSII subcomplexes could represent two distinct forms of the PSII RCa complex identified by Komenda et al. (2008). The YCF48 protein was present in high amounts in mutants lacking the Sll0218 protein. YCF48 is an important PSII assembly factor which optimizes the assembly of the RC complex by stabilizing the newly synthesized pD1 and its following interaction with the D2-Cyt $b_{559}$ complex (Komenda et al., 2008). Likewise, YCF48 contributes to the replacement of the damaged D1 during the PSII repair process (Komenda et al., 2008). The localization of YCF48 to both the PDM fractions and TM fractions (Fig. 6D and Rengstl et al., 2011) correlates with its role in both PSII assembly and repair. Differences in the early assembly steps are likely reflected in poor accumulation of PSII dimers in the absence of Sll0218 (Zhang et al., 2012), and conversely, in relatively low amounts of CP47-RC assembly intermediate complexes in the *flv4-2* operon OE mutant (Chukhutsina et al., 2015). The PSII assembly problems and accumulation of PSII-YCF48 assembly intermediates, occurring specifically in the absence of Sll0218, suggest a key role for the Sll0218 protein in stabilization of the early PSII assembly intermediates and consequently also for the formation and accumulation of PSII monomer and dimer complexes.

Interestingly, Δ*sll0218-flv2* and Δ*sll0218* mutants also revealed an impaired accumulation of a stomatin-like protein, called Phb3, which forms a ring-like assembly with a diameter of ~16 nm (Boehm et al., 2009) and has been localized to the PSII repair zones of the membrane (Sacharz et al., 2015). Proteins of the stomatin family might have a scaffold function in the organization of the membrane (Browman et al., 2007). Cyanobacterial thylakoid biogenesis centers, with particular focus on PSII assembly and repair, have been under extensive research during the past ten years (van de Meene et al., 2006; Rengstl et al., 2011; Stengel et al., 2012; Heinz et al., 2016). Localization of Sll0218 by confocal microscopy to definite spots at the peripheral side of TM (Figure 6A-B-C) together with independent membrane fractionation studies (Figure 6D) that selectively detected the Sll0218 protein in the PDM fractions, provided compelling evidence that the Sll0218 protein is an integral component of the thylakoid biogenesis centers. Interestingly, Sll0218 specifically localizes to PDM fractions while YCF48 localizes to both PDM

and TM fractions, probably suggesting a role of Sll0218 in the stabilization of early stages of PSII assembly, while YCF48 is likely to act in both the assembly and repair processes (Komenda et al., 2008). In some cases, the fusion of a relatively small hydrophobic protein to a much larger hydrophilic YFP could hamper its mobility with a possibility that the fusion product is found exclusively at the periphery of the cell, whereas the native functional protein is localized differently. However, Sll0218 is localized to the membrane fraction and it forms a high molecular mass complex which can be detected by immunoblotting of native gels loaded with the membrane extract of *Synechocystis* cells (Zhang et al., 2012). Therefore, in accordance with the membrane fractionation studies (Fig. 6D) which put Sll0218 in the PDM fractions (PDM areas localize at the periphery of the cells as shown by immunogold labelling by Stengel et al., 2012), it is unlikely that the observed Sll0218-YFP fluorescence from the membrane region of the cells would be an artefact.

The lack of Sll0218 also has indirect consequences observed as phycobilisome antenna detachment. This phenomenon was previously reported in *flv4-2* operon mutants, together with a concomitant relative decrease of PSII dimers in the Δ*flv4* mutant (Chukhutsina et al., 2015). The phycobilisome detachment in the *flv4-2* operon mutants was visualized by an increase of the F685 peak in steady-state fluorescence emission spectra at 77K (Zhang et al., 2012; Bersanini et al., 2014), and the effect was proposed to be related to the lack of Sll0218, as a consequence of PSII dimer destabilization (Chukhutsina et al., 2015). This assumption, however, lacked direct evidence in the absence of suitable mutants for experimentation. Use of the Δ*sll0218* mutant finally provided direct proof and indicated that the enhanced 77K fluorescence emission at F685 results from the absence of Sll0218 (Figure 7). Thus, the absence of Sll0218, via destabilization of PSII, is responsible also for the antenna detachment.

**Concerted action of Flv2/Flv4 and Sll0218 enables efficient PSII accumulation and function**

The expression of the Flv2 and Flv4 proteins, and their function as a Flv2/Flv4 heterodimer, is a prerequisite for the maintenance of PSII activity, as evidenced by the fact that the *flv4-2* operon mutants Δ*flv2,* Δ*sll0218-flv2 and* Δ*flv4* display malfunction of PSII electron transfer (Figure 2B). Conversely, the absence of the Sll0218 protein (Δ*sll0218*) (Figure 2B) did not affect the functionality of existing PSII

centers but severely destabilized the early assembly/repair intermediates of PSII. Thus, the dual role of the *flv4-2* operon encoded proteins in turnover of the PSII centers, firstly by alleviating the electron pressure in the ETC (Flv2/Flv4) and secondly, by providing stability for PSII early assembly intermediates (Sll0218) calls for coordinated expression of the proteins in the operon. Strong transcriptional regulation of the operon by antisense RNAs (Eisenhut et al., 2012) guarantees controlled expression of the operon when environmental conditions change and PSII needs efficient protection. Both protection mechanisms are important for optimal maintenance of PSII under ambient $CO_2$ levels.

Maintenance of PSII centers even in GL, as deduced from the amount of the D1 protein, is severely impaired in the absence of Sll0218 (50% less than in WT), while in the absence of Flv2/Flv4 the D1 protein accumulation is less compromised, only by about 30% (Figure 2A; Zhang et al., 2012). As demonstrated by the Δ*sll0218* mutant, the function of Flv2/Flv4 in alleviation of electron accumulation in ETC only partially helps in keeping the PSII complexes at optimal level. In GL, the presence of Flv2/Flv4 in the Δ*sll0218* mutant significantly improved the maintenance of PSII activity compared to the Δ*sll0218-flv2* mutant, whereas at HL the presence of Flv2/Flv4 failed to rescue the photosensitive phenotype, as happened also for Δ*sll0218-flv2* and Δ*flv4* (Figure 3). Thus, the exposure of cells to increasing light intensities, with concomitant enhancement of the PSII assembly/repair cycle, makes Sll0218 the most indispensable protein encoded by the *flv4-2* operon.

**ACKNOWLEDGEMENTS**

This work was supported by the Alfred Kordelin Foundation and by the Academy of Finland Projects (N° 271832; N° 273870; N° 272424). The following projects are also acknowledged: PHOTOCOMM (ITN, 317184), CALIPSO (ITN, 607607), TEKES (LIF 40128/14), NKFI-H (NN-110960), and SOLARH2 (N° 212508). Work in the Nickelsen lab was supported by the DFG Research Unit FOR2092 (Ni390/9) and by LMU Munich's Institutional Strategy LMUexcellent within the framework of the German Excellence Initiative. Dr J. Komenda is acknowledged for sharing the Δ*ycf48* and Δ*ycf48/sll0933* strains.

**CONFLICT OF INTEREST**

The authors declare no conflict of interest.

## REFERENCES


Acuña A.M., Snellenburg J.J., Gwizdala M., Kirilovsky D., van Grondelle R. & van Stokkum I.H. (2015) Resolving the contribution of the uncoupled phycobilisomes to cyanobacterial pulse-amplitude modulated (PAM) fluorometry signals. *Photosynthesis Research* 127, 91-102.

Allahverdiyeva Y., Ermakova M., Eisenhut M., Zhang P., Richaud P., Hagemann M., …, Aro EM. (2011) Interplay between flavodiiron proteins and photorespiration in *Synechocystis* sp. PCC 6803. *Journal of Biological Chemistry* 286: 24007-24014.

Allahverdiyeva Y., Mustila H., Ermakova M., Bersanini L., Richaud P., Ajlani G., ..., Aro EM. (2013) Flavodiiron proteins Flv1 and Flv3 enable cyanobacterial growth and photosynthesis under fluctuating light. *Proceedings of the National Academy of Sciences USA* 110, 4111-4116.

Armbruster U., Zühlke J., Rengstl B., Kreller R., Makarenko E., Rühle T., …, Leister D. (2010) The *Arabidopsis* thylakoid protein PAM68 is required for efficient D1 biogenesis and photosystem II assembly. *The Plant Cell* 22, 3439-3460.

Aro EM., Virgin I. & Andersson B. (1993) Photoinhibition of photosystem II. Inactivation, protein damage and turnover. *Biochimica et Biophysica Acta* 1143: 113-134.

Aro EM., Suorsa M., Rokka A., Allahverdiyeva Y., Paakkarinen V., Saleem A., ..., Rintamäki E. (2005) Dynamics of photosystem II: a proteomic approach to thylakoid protein complexes. *Journal of Experimental Botany* 56, 347-356.

Badger M.R. & Price G.D. (2003) $CO_2$ concentrating mechanisms in cyanobacteria: molecular components, their diversity and evolution. *Journal of Experimental Botany* 54, 609-622.

Birungi M., Folea M., Battchikova N., Xu M., Mi H., Ogawa T., …, Boekema E.J. (2010) Possibilities of subunit localization with fluorescent protein tags and electron microscopy examplified by a cyanobacterial NDH-1 study. *Biochimica et Biophysica Acta* 1797, 1681-1686.

Boehm M., Nield J., Zhang P., Aro E.M., Komenda J. & Nixon P.J. (2009) Structural and mutational analysis of band 7 proteins in the cyanobacterium *Synechocystis* sp strain PCC 6803. *Journal of Bacteriology* 191, 6425-6435.

Bersanini L., Battchikova N., Jokel M., Rehman A., Vass I., Allahverdiyeva Y. & Aro EM. (2014) Flavodiiron protein Flv2/Flv4-related photoprotective mechanism dissipates excitation pressure of PSII in cooperation with phycobilisomes in cyanobacteria. *Plant Physiology* 164, 805-818.

Browman D.T., Hoegg M.B. & Robbins S.M. (2007) The SPFH domain-containing proteins: more than lipid raft markers. *Trends in Cell Biology* 17, 394-402.

Campbell D., Hurry V., Clarke A.K., Gustafsson P. & Oquist G. (1998) Chlorophyll fluorescence analysis of cyanobacterial photosynthesis and acclimation. *Microbiology and Molecular Biology Reviews* 62, 667-683.

Chukhutsina V., Bersanini L., Aro EM. & van Amerongen H. (2015) Cyanobacterial *flv4-2* operon-encoded proteins optimize light-harvesting and charge separation in photosystem II. *Molecular Plant* 8, 747-761.

Eisenhut M., Georg J., Klähn S., Sakurai I., Mustila H., Zhang P., ..., Aro EM. (2012) The antisense RNA As1_flv4 in the cyanobacterium *Synechocystis* sp. PCC 6803 prevents premature expression of the *flv4-2* operon upon shift in inorganic carbon supply. *Journal of Biological Chemistry* 287, 33153-33162.

Ermakova M., Battchikova N., Allahverdiyeva Y. & Aro EM. (2013) Novel heterocyst-specific flavodiiron proteins in *Anabaena* sp. PCC 7120. *FEBS Letters* 587, 82-87.

499 Ermakova M., Battchikova N., Richaud P., Leino H., Kosourov S., Isojärvi J., …, Aro EM. (2014) Heterocyst-
500 specific flavodiiron protein Flv3B enables oxic diazotrophic growth of the filamentous
501 cyanobacterium *Anabaena* sp. PCC 7120. *Proceedings of the National Academy of Sciences USA*
502 111, 11205-11210.

503 Gehl B. & Sweetlove L.J. (2014) Mitochondrial Band-7 family proteins: scaffolds for respiratory chain
504 assembly? Frontiers in Plant Science 5, 141.

505 Hackenberg C., Engelhardt A., Matthijs H.C., Wittink F., Bauwe H., Kaplan A. & Hagemann M. (2009)
506 Photorespiratory 2-phosphoglycolate metabolism and photoreduction of $O_2$ cooperate in high-
507 light acclimation of *Synechocystis* sp. strain PCC 6803. *Planta* 230, 625-637.

508 Hakkila K., Antal T., Gunnelius L., Kurkela J., Matthijs H.C.P., Tyystjärvi E. & Tyystjärvi T. (2013) Group 2
509 sigma factor mutant ΔsigCDE of the cyanobacterium *Synechocystis* sp. PCC 6803 reveals
510 functionality of both carotenoids and flavodiiron proteins in photoprotection of photosystem II.
511 *Plant and Cell Physiology* 54, 1780-1790.

512 Heinz S., Liauw P., Nickelsen J. & Nowaczyk M. (2016) Analysis of photosystem II biogenesis in
513 cyanobacteria. *Biochimica et Biophysica Acta* 1857, 274-287.

514 Helman Y., Tchernov D., Reinhold L., Shibata M., Ogawa T., Schwarz R., …, Kaplan A. (2003) Genes
515 encoding A-type flavoproteins are essential for photoreduction of $O_2$ in cyanobacteria. Current
516 Biology 13, 230-235.

517 Järvi S., Suorsa M. & Aro EM. (2015) Photosystem II repair in plant chloroplasts - regulation, assisting
518 proteins and shared components with photosystem II biogenesis. *Biochimica et Biophysica Acta*
519 1847(9), 900-909.

520 Jokel M., Kosourov S., Battchikova N., Tsygankov A.A., Aro EM. & Allahverdiyeva Y. (2015) *Chlamydomonas*
521 flavodiiron proteins facilitate acclimation to anoxia during sulfur deprivation. *Plant and Cell*
522 *Physiology* 56, 1598-1607.

523 Kaplan A. & Reinhold L. (1999) $CO_2$ concentrating mechanisms in photosynthetic microorganisms.
524 *Annual Reviews in Plant Physiology and Plant Molecular Biology* 50, 539-570.

525 Knoppová J., Sobotka R., Tichý M., Yu J., Konik P., Halada P., …, Komenda J. (2014) Discovery of a
526 chlorophyll binding protein complex involved in the early steps of photosystem II assembly in
527 *Synechocystis*. *The Plant Cell* 26, 1200-1212.

528 Komenda J., Nickelsen J., Tichy M., Prasil O., Eichacker L.A. & Nixon P.J. (2008) The cyanobacterial
529 homologue of HCF136/YCF48 is a component of an early photosystem II assembly complex and
530 is important for both the efficient assembly and repair of photosystem II in *Synechocystis* sp. PCC
531 6803. *Journal of Biological Chemistry* 283, 22390-99.

532 Komenda J., Sobotka R. & Nixon P.J. (2012) Assembling and maintaining the photosystem II complex in
533 chloroplasts and cyanobacteria. *Current Opinion in Plant Biology* 15, 245-251.

534 Laemmli U.K. (1970) Cleavage of structural proteins during the assembly of the head of bacteriophage
535 T4. *Nature* 227, 680-685.

536 Lagarde D., Beuf L. & Vermaas W. (2000) Increased production of zeaxanthin and other pigments by
537 application of genetic engineering techniques to *Synechocystis* sp. strain PCC 6803. *Applied*
538 *Environmental Microbiology* 66, 64-72.

539 Mabbitt P.D., Wilbanks S.M. & Eaton-Rye J.J. (2014) Structure and function of the hydrophilic
540 Photosystem II assembly proteins: Psb27, Psb28 and Ycf48. *Plant Physiology and Biochemistry* 81,
541 96-107.

542 Mackenzie T.D., Burns R.A. & Campbell D.A. (2004) Carbon status constrains light acclimation in the
543 cyanobacterium *Synechococcus elongatus*. *Plant Physiology* 136, 3301-3312.

544 Meeks J.C. & Castenholz R.W. (1971) Growth and photosynthesis in an extreme thermophile
545 *Synechococcus lividus* (Cyanophyta). *Archives fur Mikrobiologie* 78, 25-41.

546 Mohamed A., Eriksson J., Osiewacz H.D., & Jansson C. (1993) Differential expression of the *psbA* genes in
547 the cyanobacterium *Synechocystis* 6803. *Molecular and General Genetics MGG* 238, 161-168.

548 Mullineaux C.W. & Sarcina M. (2002) Probing the dynamics of photosynthetic membranes with
549 fluorescence recovery after photobleaching. *Trends in Plant Science* 7, 237-240.

550 Mustila H., Paananen P., Battchikova N., Santana-Sanchez A., Muth-Pawlak D., Hagemann M., …,
551 Allahverdiyeva Y. (2016) The flavodiiron protein Flv3 functions as a homo-oligomer during stress
552 acclimation and is distinct from the Flv1/Flv3 hetero-oligomer specific to the $O_2$ photoreduction
553 pathway. *Plant and Cell Physiology* http://dx.doi.org/10.1093/pcp/pcw047.

554 Nickelsen J. & Rengstl B. (2013) Photosystem II assembly: from cyanobacteria to plants. *Annual Reviews*
555 *in Plant Biology* 64, 609-635.

556 Nishiyama Y. & Murata N. (2014) Revised scheme for the mechanism of photoinhibition and its
557 application to enhance the abiotic stress tolerance of the photosynthetic machinery. *Applied*
558 *Microbiology and Biotechnology* 98, 8777-8796.

559 Ossenbühl F., Inaba-Sulpice M., Meurer J., Soll J. & Eichacker L.A. (2006) The *Synechocystis* sp PCC 6803
560 Oxa1 homolog is essential for membrane integration of reaction center precursor protein pD1.
561 *The Plant Cell* 18, 2236-2246.

562 Price G.D., Badger M.R., Woodger F.J. & Long B.M. (2008) Advances in understanding the cyanobacterial
563 $CO_2$-concentrating-mechanism (CCM): functional components, $C_i$ transporters, diversity, genetic
564 regulation and prospects for engineering into plants. *Journal of Experimental Botany* 59, 1441-
565 1461.

566 Rengstl B., Oster U., Stengel A. & Nickelsen J. (2011) An intermediate membrane subfraction in
567 cyanobacteria is involved in an assembly network for photosystem II biogenesis. *Journal of*
568 *Biological Chemistry* 286, 21944‑21951.

569 Rengstl B., Knoppová J., Komenda J. & Nickelsen J. (2013) Characterization of a *Synechocystis* double
570 mutant lacking the photosystem II assembly factors YCF48 and Sll0933. *Planta* 237, 471-80.

571 Sacharz J., Bryan S.J., Yu J., Burroughs N.J., Spence E.M., Nixon P.J. & Mullineaux C.W. (2015) Sub-cellular
572 location of FtsH proteases in the cyanobacterium *Synechocystis* sp. PCC 6803 suggests localised
573 PSII repair zones in the thylakoid membranes, *Molecular Microbiology* 96, 448-462.

574 Schottkowski M., Gkalympoudis S., Tzekova N., Stelljes C., Schünemann D., Ankele E. & Nickelsen J.
575 (2009a) Interaction of the periplasmic PratA factor and the PsbA (D1) protein during biogenesis
576 of photosystem II in *Synechocystis* sp. PCC 6803. *Journal of Biological Chemistry* 284, 1813-1819.

577 Schottkowski M., Ratke J., Oster U., Nowaczyk M. & Nickelsen J. (2009b) Pitt, a novel tetratricopeptide
578 repeat protein involved in light-dependent chlorophyll biosynthesis and thylakoid membrane
579 biogenesis in *Synechocystis* sp. PCC 6803. *Molecular Plant* 2, 1289-1297.

580 Stengel A., Gügel I.L., Hilger D., Rengstl B., Jung H. & Nickelsen J. (2012) Initial steps of photosystem II de
581 novo assembly and preloading with manganese take place in biogenesis centers in
582 *Synechocystis*. *The Plant Cell* 24, 660-675.

583 van de Meene A., Hohmann-Marriott M., Vermaas W. & Roberson R. (2006) The three-dimensional
584 structure of the cyanobacterium *Synechocystis* sp. PCC 6803. *Archives of Microbiology* 184, 259-
585 70.

586 Vicente J.B., Carrondo M.A., Teixeira M. & Frazão C. (2008a) Structural studies on flavodiiron proteins.
587 *Methods in Enzymology* 437, 3-19.

588 Vicente J.B., Justino M.C., Gonçalves V.L., Saraiva L.M. & Teixeira M. (2008b) Biochemical, spectroscopic,
589 and thermodynamic properties of flavodiiron proteins. *Methods in Enzymology* 437, 21-45.

590 Vicente J.B., Testa F., Mastronicola D., Forte E., Sarti P., Teixeira M. & Giuffrè A. (2009) Redox properties of
591 the oxygen-detoxifying flavodiiron protein from the human parasite *Giardia intestinalis*. *Archives*
592 *of Biochemistry and Biophysics* 488, 9-13.

593 Wasserfallen A., Ragettli S., Jouanneau Y. & Leisinger T. (1998) A family of flavoproteins in the domains
594 Archaea and Bacteria. *European Journal of Biochemistry* 254, 325-332.

595 Westphal S., Heins L., Soll J. & Vothknecht U.C. (2001) *Vipp1* deletion mutant of *Synechocystis*: a
596 connection between bacterial phage shock and thylakoid biogenesis? *Proceedings of the*
597 *National Academy of Sciences USA* 98, 4243-48.

598 Williams J.G.K. (1988) Construction of specific mutations in photosystem II photosynthetic reaction
599 center by genetic engineering methods in *Synechocystis* 6803. *Methods in Enzymology* 167, 766-
600 778.

601 Zhang P., Allahverdiyeva Y., Eisenhut M. & Aro EM. (2009) Flavodiiron proteins in oxygenic
602 photosynthetic organisms: Photoprotection of photosystem II by Flv2 and Flv4 in *Synechocystis*
603 sp. PCC 6803. *PLoS ONE* 4, e5331.

604 Zhang P., Eisenhut M., Brandt A.M., Carmel D., Silén H.M., Vass I., ..., Aro EM. (2012) Operon *flv4-flv2*
605 provides cyanobacterial photosystem II with flexibility of electron transfer. *The Plant Cell* 24,
606 1952-1971.

607 **FIGURE LEGENDS**

608 **Figure 1.** Phenotypes of different *flv4-2* operon mutants. **A.** Immunoblot analysis of Flv4, Sll0218 and
609 Flv2. An amount of 40 µg of proteins was loaded for each strain. **B.** Color phenotype of strains grown in
610 HL for 6 days. **C.** Chl *a* content of cultures grown in GL and HL determined with methanol extraction and
611 normalized to $OD_{750}$ (means ± SD of three independent experiments). Black and red asterisks indicate
612 statistically significant difference compared respectively to the WT GL values (Student t-test, P<0.01) and
613 to WT HL values (Student t-test, P<0.05).

614 **Figure 2.** Accumulation of thylakoid proteins and comparison of PSII activities of the *flv4-2* operon
615 mutants. **A.** Immunoblot analysis with antibodies to representative proteins of different photosynthetic
616 complexes. The gels were loaded with 20µg of proteins. The D1 protein quantification was performed
617 with a GeneTool software (PerkinElmer) from three biological replicates (maximum SD of ± 15%). **B.** PSII
618 activities determined as oxygen evolution rates in the presence of 2mM DMBQ with saturating light (WT
619 value: 390 ± 41 µmol $O_2$ mg of $Chl^{-1}$ $h^{-1}$), and PSII yield, Y(II), of cells exposed to red actinic light of 120
620 µmol photons $m^{-2}$ $s^{-1}$ for 2 minutes through PAM fluorimetry (WT value: 0.19 ± 0.02). The cultures were
621 adjusted to same Chl concentration before the measurements. Values are means ± SD of four
622 independent experiments. Black asterisks and black open circles: statistically significant difference of the
623 PSII activity values of a respective strain compared to WT values (Student t-test, P<0.05). Red asterisk and
624 red open circle: statistically significant difference of the PSII activity values of Δ*sll0218* strain compared
625 to Δ*sll0218-flv2* (Student t-test, P<0.05).

626 **Figure 3.** Time course of PSII photoinhibition in WT and *flv4-2* operon mutants exposed to white light
627 with intensity of 1000 µmol photons $m^{-2}$ $s^{-1}$ in the absence ( - LIN) and presence (+ LIN) of lincomycin
628 (300 µg $mL^{-1}$). Oxygen evolution rates were measured in the presence of 2mM DMBQ. The cultures were
629 adjusted to a Chl concentration of 10 µg $mL^{-1}$. Values are means ± SD of three independent experiments.
630 Asterisks indicate statistically significant difference of the oxygen evolution rates measured at 90 min for
631 the Δ*sll0218-flv2*, Δ*flv4* and Δ*sll0218* strains compared to WT values (Student t-test, P<0.05).

**Figure 4.** Accumulation of PSII intermediates in WT, Δ*sll0218* and Δ*sll0218-flv2* strains. **A.** The BN-PAGE gel was loaded with 100µg of proteins and analyzed by further immunoblotting with D1 and YCF48 antibodies. The yellow arrows indicate the RC* complex identified by Komenda et al. (2008) and Rengstl et al. (2013). The red arrows indicate protein complexes that accumulate in Δ*sll0218* and Δ*sll0218-flv2* strains, and possibly correspond to the PSII RCa complex forms demonstrated by (Komenda et al., 2008). **B.** Protein complexes from the red rectangle indicated in the BN-gel in A were run by SDS/PAGE in the 2$^{nd}$ dimension and immunoblotted with D1 and YCF48 antibodies. The complexes indicated in A by yellow and red arrows were identified by immunoblotting with D1 and YCF48 antibodies and are indicated with similar arrows in B. The intermediate form of D1 (iD1) could also be identified in the complexes.

**Figure 5. A.** Immunoblot demonstrating the accumulation of different PSII assembly-related factors in the *flv4-2* operon mutants (see details in the text). The gels were loaded with 20µg of proteins. The YCF48 protein quantification was achieved with a GeneTool (PerkinElmer) software from three biological replicates (maximum SD of ± 15%). **B.** Accumulation of *flv4-2* operon-encoded proteins in WT, Δ*ycf48*, Δ*sll0933* and Δ*ycf48/sll0933* strains detected by immunoblotting the gels loaded with 20 µg of protein. **C.** Accumulation of *flv4-2* operon-encoded proteins in WT, Δ*ycf48* and Δ*ycf48/sll0933* strains detected by immunoblotting the gels loaded with an amount of protein normalized to the D1 content, making use of the quantification of D1 content obtained in B.

**Figure 6.** Localization of the Sll0218 protein. **A.** A confocal fluorescence image of *Synechocystis* Sll0218-YFP cells, showing merged YFP fluorescence with chlorophyll fluorescence (YFP in green, chlorophyll in red) for cells grown in GL. **B.** Sll0218-YFP spot numbers per cell ± SEM (n = 250). **C.** Averaged fluorescence radial distributions (*n* = 30) normalized to cell radius. Red lines indicate chlorophyll fluorescence profile ± SD, blue lines indicate YFP fluorescence profile ± SD. **D.** Localization of Sll0218 in the PDM fraction. *Synechocystis* cell extracts of the WT strain were separated by two consecutive rounds of sucrose density gradient centrifugation. The second linear gradient from 20 to 60% sucrose was divided into 14 fractions followed by immunoblotting with indicated antibodies. Fractions 1-6 represent PDMs, fractions 7-14

658 represent TMs. Sample volumes were normalized to the volume of fraction 7 that contained 40µg of
659 protein.

660 **Figure 7.** The 77K steady-state fluorescence emission spectra of the *flv4-2* operon mutants induced by
661 excitation with 580 nm light. The spectra were averaged from at least three independent experiments.
662 Each spectrum was normalized to PSI fluorescence peak at 723 nm.

**FiGURES**

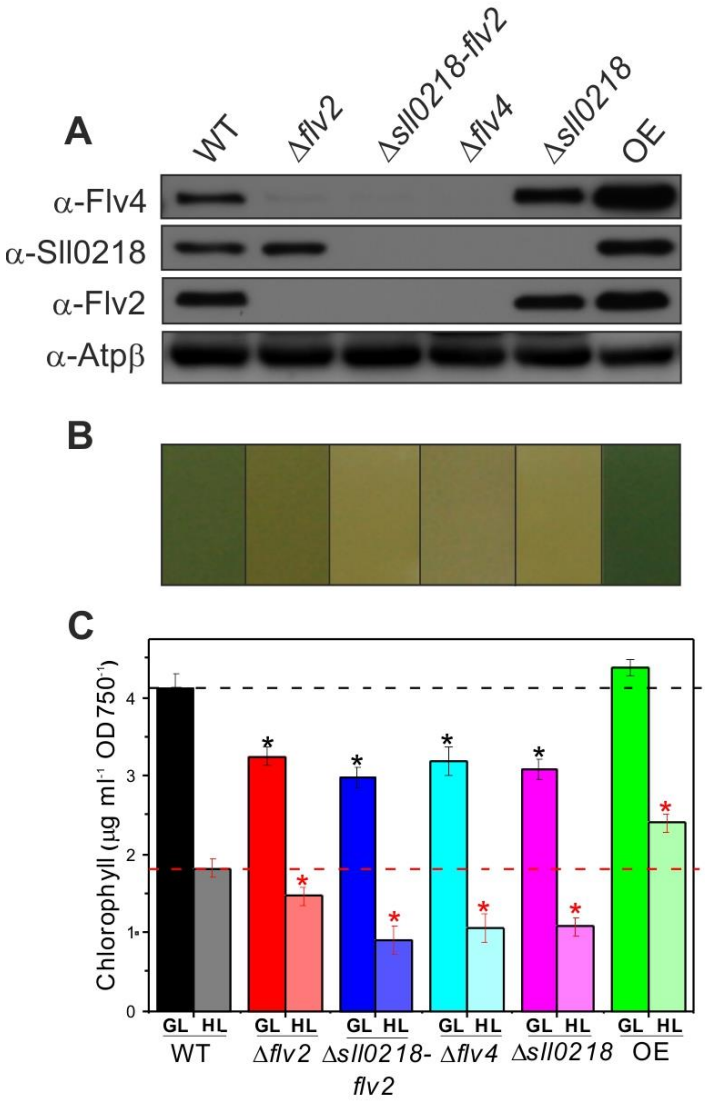


**Figure 1.** Phenotypes of different *flv4-2* operon mutants. **A.** Immunoblot analysis of Flv4, Sll0218 and Flv2. An amount of 40 µg of proteins was loaded for each strain. **B.** Color phenotype of strains grown in HL for 6 days. **C.** Chl *a* content of cultures grown in GL and HL determined with methanol extraction and normalized to $OD_{750}$ (means ± SD of three independent experiments). Black and red asterisks indicate statistically significant difference compared respectively to the WT GL values (Student t-test, $P<0.01$) and to WT HL values (Student t-test, $P<0.05$).

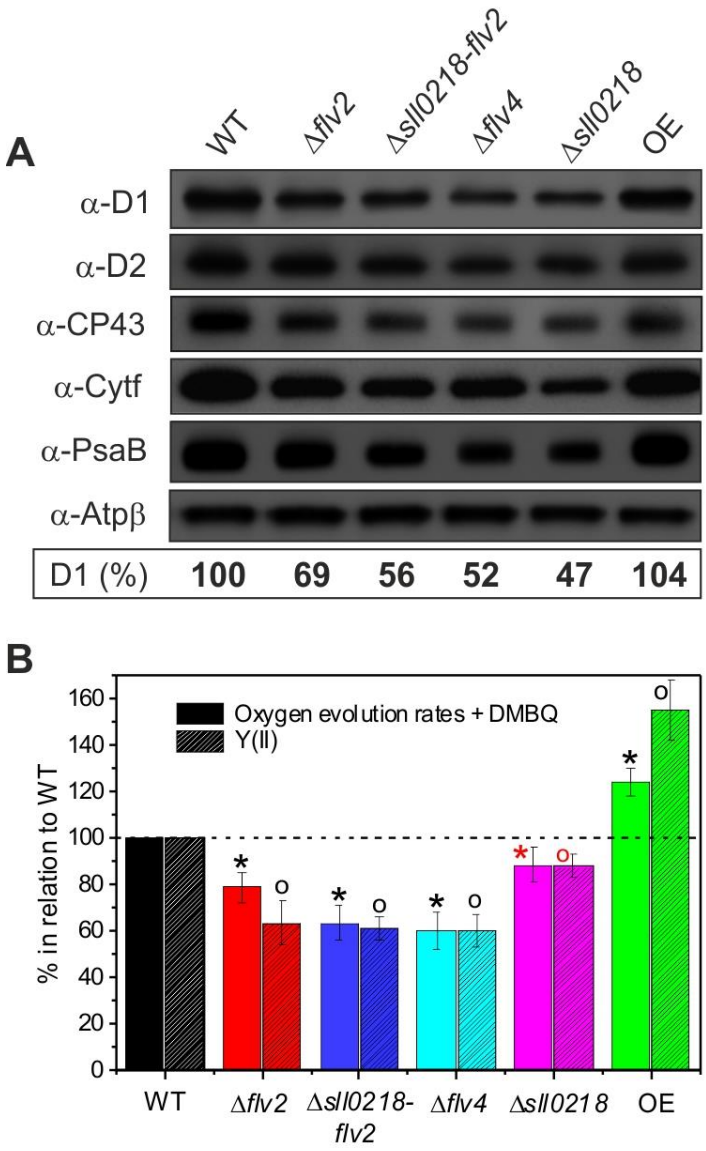


**Figure 2.** Accumulation of thylakoid proteins and comparison of PSII activities of the *flv4-2* operon mutants. **A.** Immunoblot analysis with antibodies to representative proteins of different photosynthetic complexes. The gels were loaded with 20µg of proteins. The D1 protein quantification was performed with a GeneTool software (PerkinElmer) from three biological replicates (maximum SD of ± 15%). **B.** PSII activities determined as oxygen evolution rates in the presence of 2mM DMBQ with saturating light (WT value: 390 ± 41 µmol $O_2$ mg of $Chl^{-1}$ $h^{-1}$), and PSII yield, Y(II), of cells exposed to red actinic light of 120 µmol photons $m^{-2}$ $s^{-1}$ for 2 minutes through PAM fluorimetry (WT value: 0.19 ± 0.02). The cultures were adjusted to same Chl concentration before the measurements. Values are means ± SD of four independent experiments. Black asterisks and black open circles: statistically significant difference of the PSII activity values of a respective strain compared to WT values (Student t-test, $P<0.05$). Red asterisk and red open circle: statistically significant difference of the PSII activity values of Δ*sll0218* strain compared to Δ*sll0218-flv2* (Student t-test, $P<0.05$).

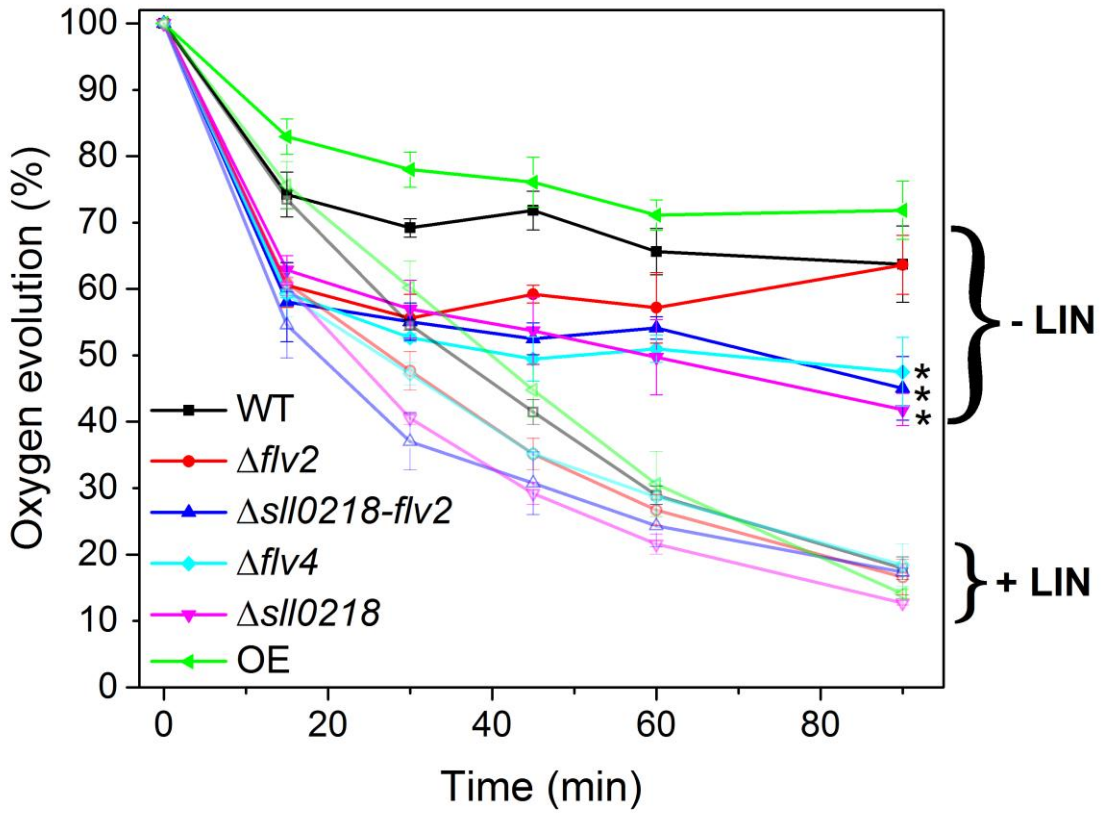


**Figure 3.** Time course of PSII photoinhibition in WT and *flv4-2* operon mutants exposed to white light with intensity of 1000 µmol photons $m^{-2}$ $s^{-1}$ in the absence ( - LIN) and presence (+ LIN) of lincomycin (300 µg $mL^{-1}$). Oxygen evolution rates were measured in the presence of 2mM DMBQ. The cultures were adjusted to a Chl concentration of 10 µg $mL^{-1}$. Values are means ± SD of three independent experiments. Asterisks indicate statistically significant difference of the oxygen evolution rates measured at 90 min for the Δ*sll0218-flv2*, Δ*flv4* and Δ*sll0218* strains compared to WT values (Student t-test, P<0.05).

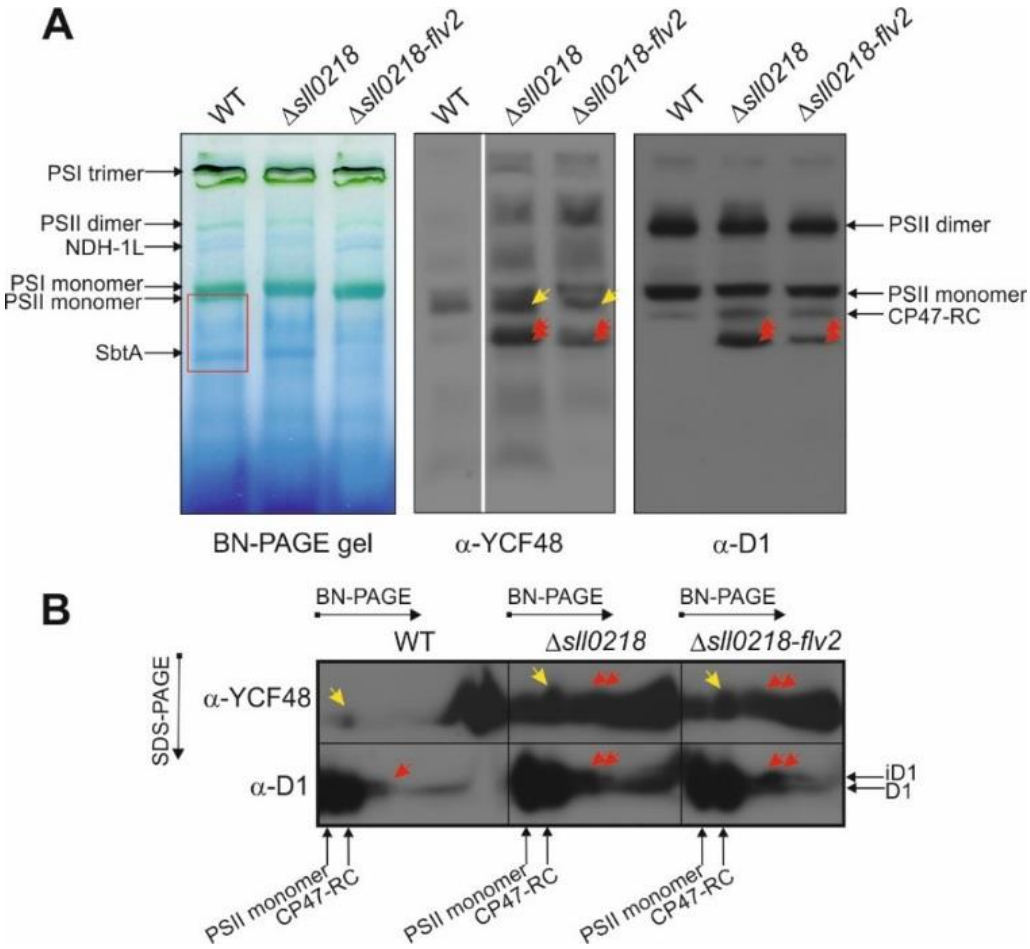


**Figure 4.** Accumulation of PSII intermediates in WT, Δ*sll0218* and Δ*sll0218-flv2* strains. **A.** The BN-PAGE gel was loaded with 100µg of proteins and analyzed by further immunoblotting with D1 and YCF48 antibodies. The yellow arrows indicate the RC* complex identified by Komenda et al. (2008) and Rengstl et al. (2013). The red arrows indicate protein complexes that accumulate in Δ*sll0218* and Δ*sll0218-flv2* strains, and possibly correspond to the PSII RCa complex forms demonstrated by (Komenda et al., 2008). **B.** Protein complexes from the red rectangle indicated in the BN-gel in A were run by SDS/PAGE in the 2nd dimension and immunoblotted with D1 and YCF48 antibodies. The complexes indicated in A by yellow and red arrows were identified by immunoblotting with D1 and YCF48 antibodies and are indicated with similar arrows in B. The intermediate form of D1 (iD1) could also be identified in the complexes.

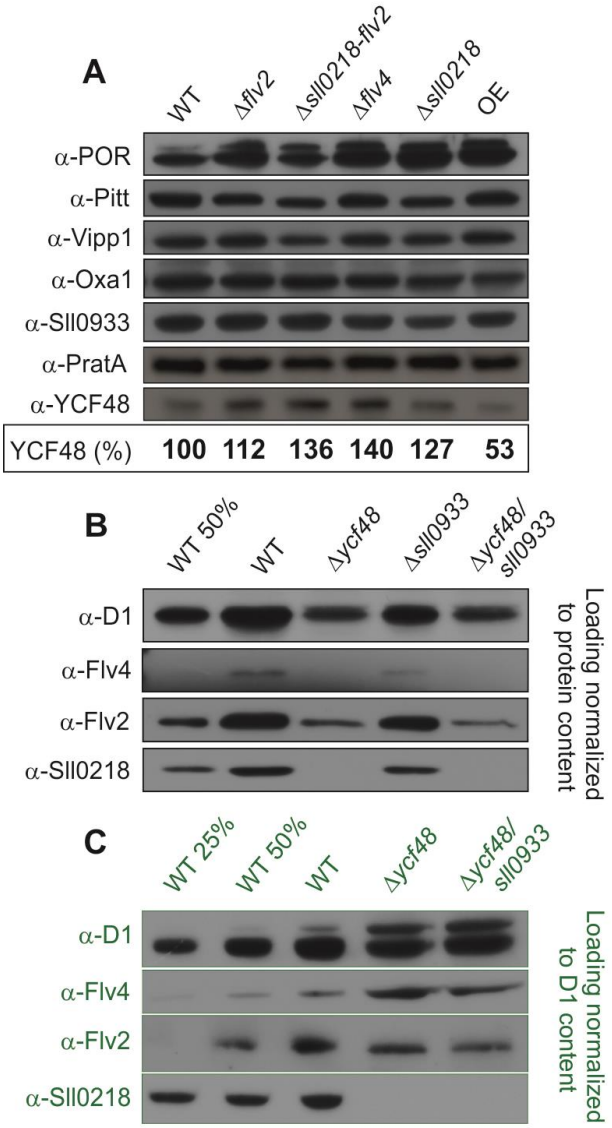


**Figure 5. A.** Immunoblot demonstrating the accumulation of different PSII assembly-related factors in the *flv4-2* operon mutants (see details in the text). The gels were loaded with 20µg of proteins. The YCF48 protein quantification was achieved with a GeneTool (PerkinElmer) software from three biological replicates (maximum SD of ± 15%). **B.** Accumulation of *flv4-2* operon-encoded proteins in WT, Δ*ycf48*, Δ*sll0933* and Δ*ycf48/sll0933* strains detected by immunoblotting the gels loaded with 20 µg of protein. **C.** Accumulation of *flv4-2* operon-encoded proteins in WT, Δ*ycf48* and Δ*ycf48/sll0933* strains detected by immunoblotting the gels loaded with an amount of protein normalized to the D1 content, making use of the quantification of D1 content obtained in B.

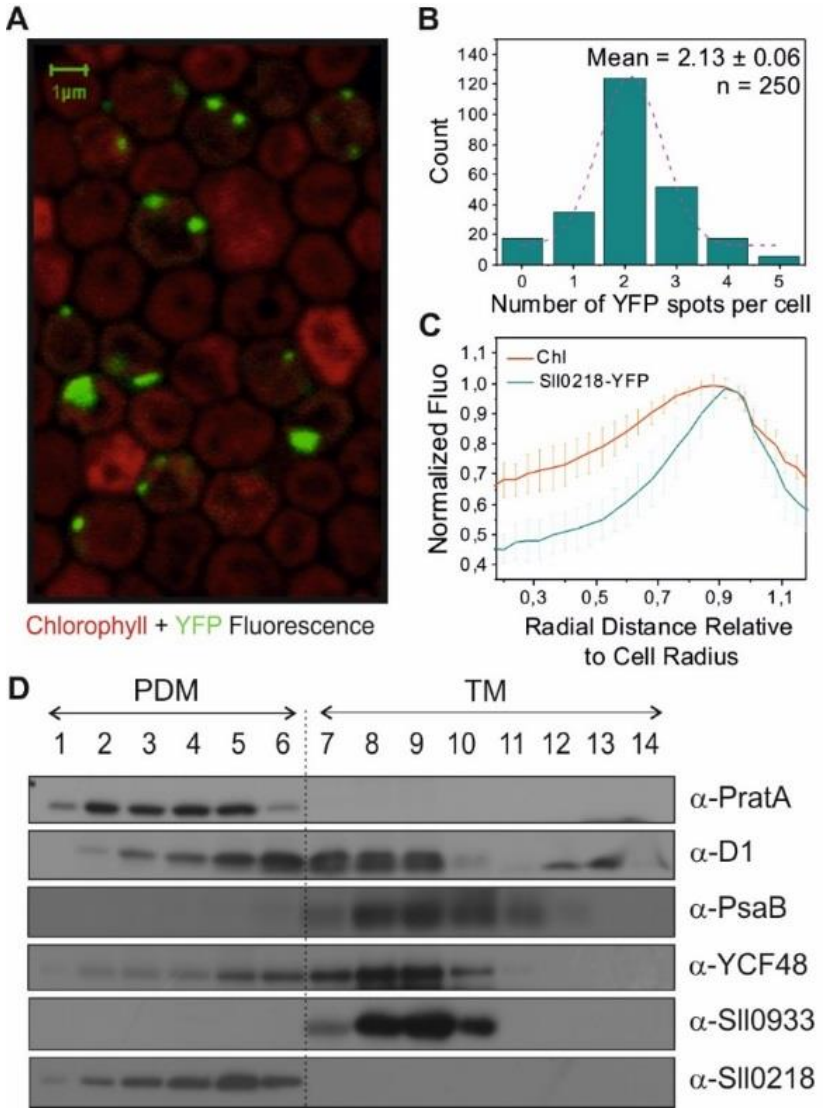


**Figure 6.** Localization of the Sll0218 protein. **A.** A confocal fluorescence image of *Synechocystis* Sll0218-YFP cells, showing merged YFP fluorescence with chlorophyll fluorescence (YFP in green, chlorophyll in red) for cells grown in GL. **B.** Sll0218-YFP spot numbers per cell ± SEM (n = 250). **C.** Averaged fluorescence radial distributions (*n* = 30) normalized to cell radius. Red lines indicate chlorophyll fluorescence profile ± SD, blue lines indicate YFP fluorescence profile ± SD. **D.** Localization of Sll0218 in the PDM fraction. *Synechocystis* cell extracts of the WT strain were separated by two consecutive rounds of sucrose density gradient centrifugation. The second linear gradient from 20 to 60% sucrose was divided into 14 fractions followed by immunoblotting with indicated antibodies. Fractions 1-6 represent PDMs, fractions 7-14 represent TMs. Sample volumes were normalized to the volume of fraction 7 that contained 40µg of protein.

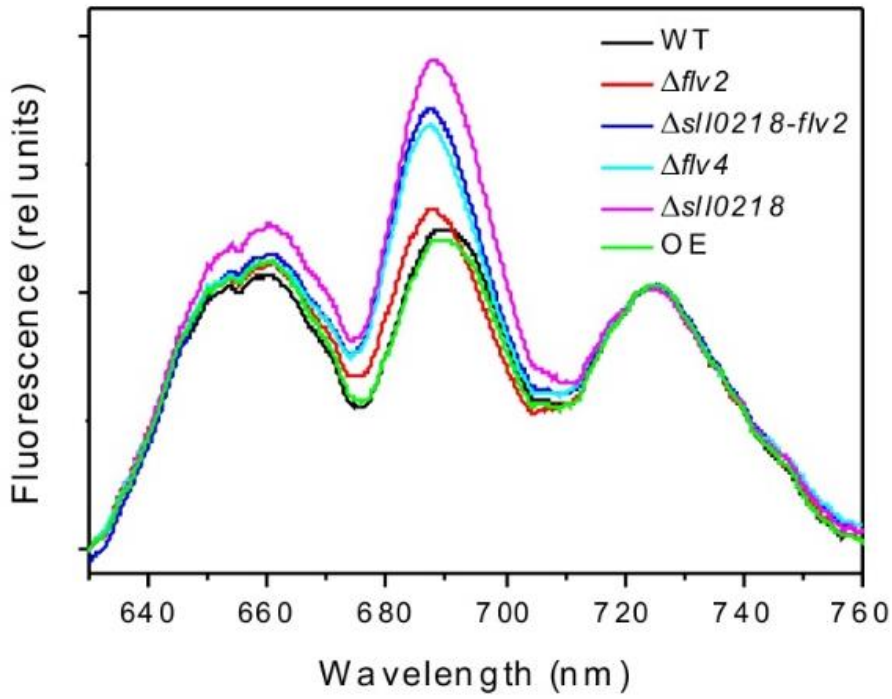


**Figure 7.** The 77K steady-state fluorescence emission spectra of the *flv4-2* operon mutants induced by excitation with 580 nm light. The spectra were averaged from at least three independent experiments. Each spectrum was normalized to PSI fluorescence peak at 723 nm.

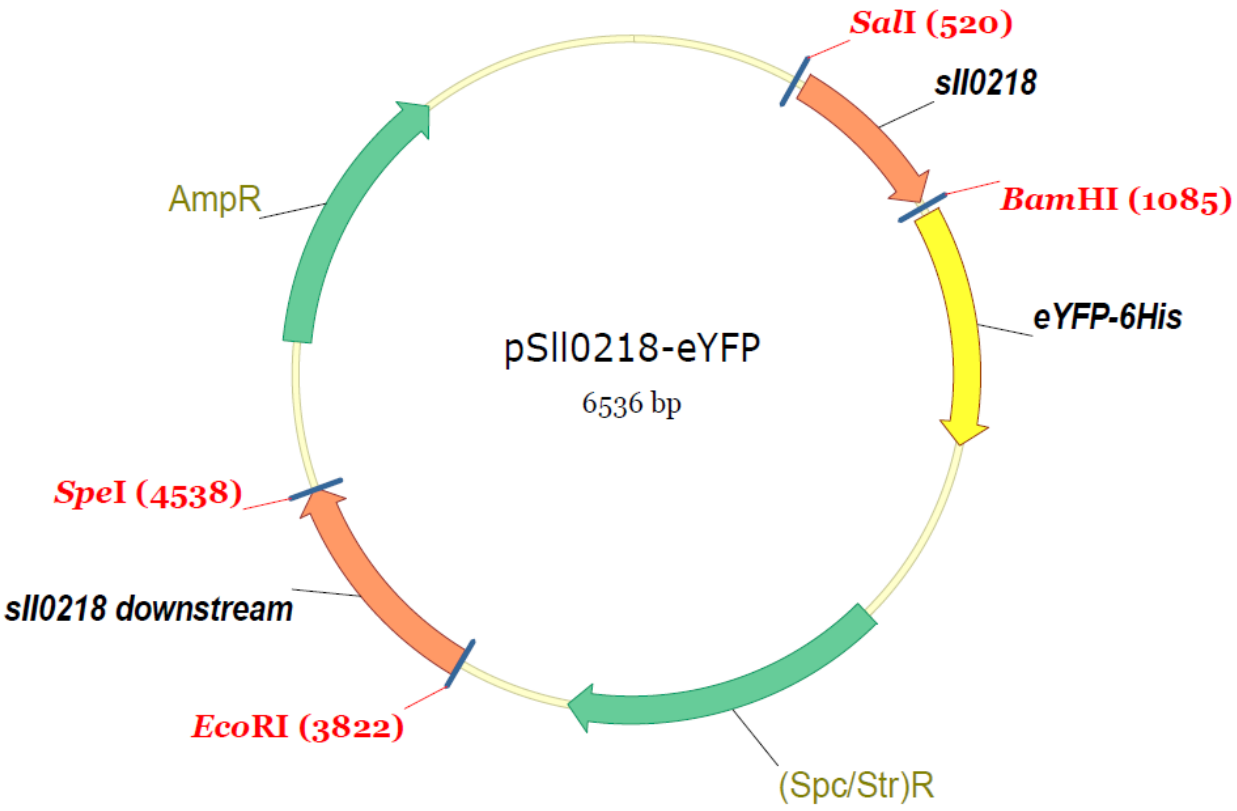


**Supplemental Figure S1.** A schematic map of the plasmid pSll0218-YFP. The *sll0218* ORF and downstream region are indicated in orange. The eYFP-6His gene is indicated in yellow. The ampicillin and spectinomycin resistance cassettes are represented in green.

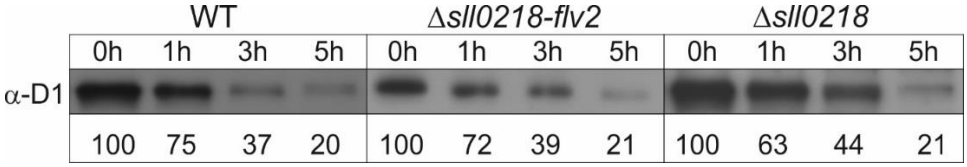


**Supplemental Figure S2.** Degradation of D1 protein in WT, Δ*sll0218* and Δ*sll0218-flv2* strains. Protein extracts of cells exposed to 1000 µmol photons $m^{-2}$ $s^{-1}$ for 1,3 and 5 hours in the presence of lincomycin (300 µg $mL^{-1}$) were equally loaded (20 µg) on SDS-PAGE gels and analyzed by immunoblotting with D1 antibodies. The D1 protein quantification was achieved with a GeneTool (PerkinElmer) software from two biological replicates (maximum SD of ± 20%).

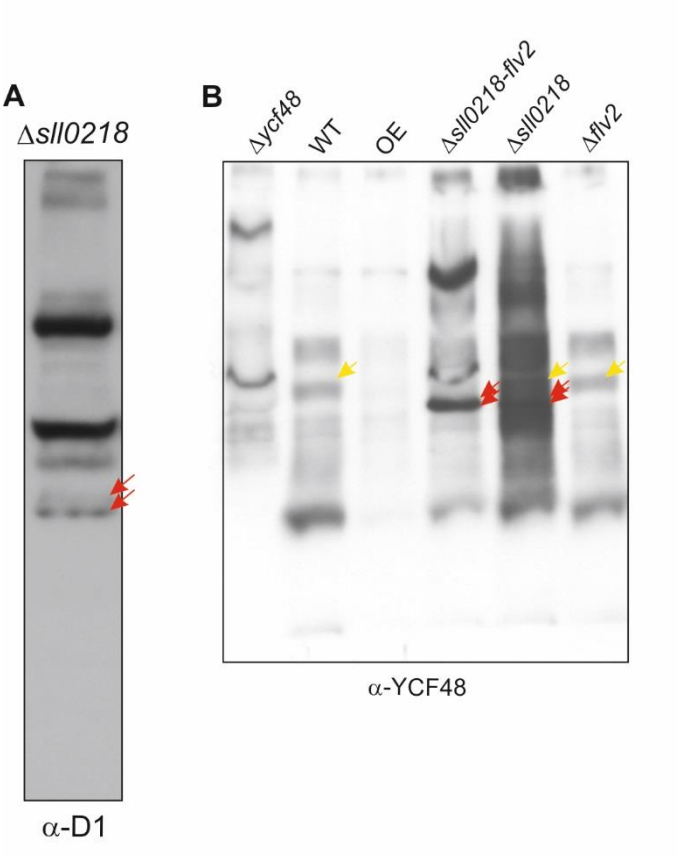


**Supplemental Figure S3. A.** Observation of two D1-containing intermediates in the Δ*sll0218* strain. Immunoblotting was performed with D1 antibody. **B.** TM complexes from WT, *flv4-2* operon mutants and the Δ*ycf48* mutant were separated by BN-PAGE (100 µg thylakoid extracts per lane) and analyzed by immunoblotting with YCF48 antibody. Red arrows indicate the D1-YCF48-containing intermediate; yellow arrows indicate the RC* complex.

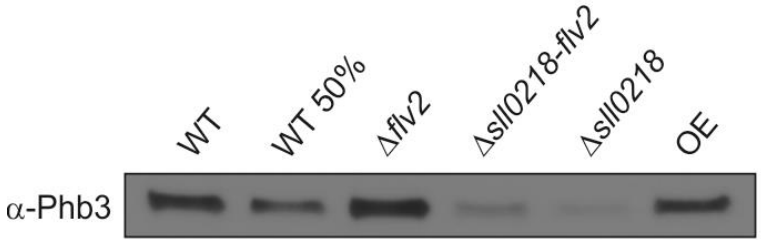


**Supplemental Figure S4.** Protein extracts (20 µg) from WT and *flv4-2* operon mutants were separated by SDS-PAGE and analyzed by immunoblotting with Phb3 (Slr1128) antibody.

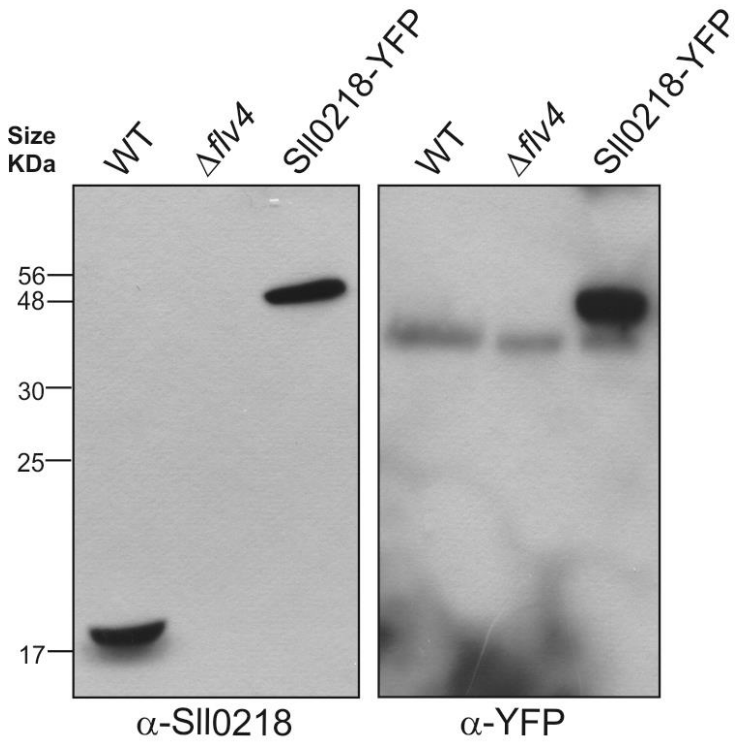


**Supplemental Figure S5.** Protein extracts (40 µg) of WT, Δ*flv4* and Sll0218-YFP strains were separated by SDS-PAGE and analyzed by immunoblotting with Sll0218 and YFP antibodies. The Sll0218-YFP fusion protein could be detected at the expected mass of about 50 KDa with both the Sll0218 and YFP antibodies.

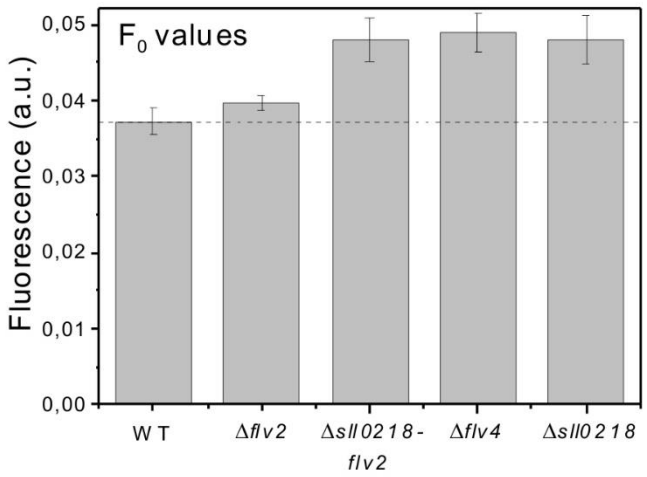


**Supplemental Figure S6.** $F_0$ values of WT and different *flv4-2* operon mutants. The $F_0$ values were obtained from PAM fluorescence induction curves. Values are means ± SD of four independent experiments.